

# Rotational damping for rapidly rotating nuclei

Lu Guo,<sup>1,\*</sup> Jie Meng,<sup>2</sup> En-Guang Zhao,<sup>3</sup> and Fumihiko Sakata<sup>4</sup>

<sup>1</sup>*Department of Mathematical Science,*

*Ibaraki University, Mito 310-8512, Ibaraki, Japan*

<sup>2</sup>*School of Physics, Peking University, Beijing 100871, China*

<sup>3</sup>*Institute of Theoretical Physics, Chinese Academy of Sciences, Beijing 100080, China*

<sup>4</sup>*Institute of Applied Beam Science,*

*Graduate School of Science and Engineering,*

*Ibaraki University, Mito 310-8512, Ibaraki, Japan*

(Dated: May 23, 2019)

## Abstract

The damping of collective rotational motion is investigated in rare-earth nucleus  $^{168}\text{Yb}$  by means of particles-rotor model. It is found that the onset energy of rotational damping is around 1.1 MeV above yrast line, and the number of levels which form rotational band structure is thus limited. The calculated number of rotational bands about 30 at a given angular momentum agrees well with experimental data. The onset of rotational damping takes place quite gradually as a function of excitation energy. It is shown that the pairing correlation between valence particles has a significant effect on the appearance of rotational damping.

PACS numbers: 21.10.Re, 23.20.Lv, 27.70.+q

---

\*Electronic address: guolu@mcs.ibaraki.ac.jp

## I. INTRODUCTION

The experimentally observed rotational bands often lie in the region near yrast line and are described as particle-hole excitations in the mean-field. At higher excitation energy above the yrast line, it does not necessarily form rotational band structure due to the damping of collective rotational motion [1, 2]. When the rotational damping takes place, E2 transition from an excited state spreads out over many final states. The gamma-rays which are emitted from the above excited region can not be distinguished as discrete peaks, thus forming a quasi-continuum spectra. Experimentally rotational damping has been studied through the analysis of quasi-continuum spectra [3, 4, 5, 6, 7]. Recent experimental progress in high precision three-dimensional gamma-ray correlation measurements makes it possible to study various features of collective rotational motion in the regions of discrete rotational bands and damped rotational motion [8, 9, 10, 11, 12, 13, 14, 15]. In particular, the newly developed fluctuation analysis method [8, 9] has presented the number of rotational bands existing in a rare-earth nucleus is only about 30 at a given angular momentum, thus confirming the occurrence of rotation damping.

Early theoretical studies on rotational damping [1, 2, 16, 17] showed that with the increase of level density the off-diagonal residual interaction becomes effective to cause mixing of many-particle many-hole configurations in the rotating mean-field. Since different configurations respond differently to the Coriolis force, the configuration mixing results in a dispersion of the rotational frequency within each energy eigenstate, implying a damping of the collective rotational motion. But in these works [1, 2, 16, 17] the assumption that the configuration mixing is described by the general statistical theory of random matrices has been used to treat the E2 strength function associated with damped rotational motion.

Recent studies on the microscopic structure and dynamics of rotational damping have been done extensively for normally deformed and superdeformed nuclei in the cranked Nilsson mean-field combined two-body residual interaction [18, 19, 20, 21, 22, 23, 24, 25]. In these discussions, the excited rotational bands are described as intrinsic many-particle many-hole excitations upon the cranked Nilsson mean-field. In order to obtain rotational damping, the bands are mixed by two-body residual interaction. However in particles-rotor model (PRM), we can use the same Hamiltonian to obtain the band structures as well as rotational damping, and to study the coupling between single-particle degree of freedom

and collective rotational motion. Moreover as noted in Ref. [19], PRM is more complete on the angular momentum coupling in wave functions and E2 transition matrix elements, since the angular momentum is not a conserved quantity in the cranked model. It should be mentioned that the connection between rotational damping and nuclear chaotic property has been addressed in Ref. [26, 27].

Different nuclear models make different approximations to the nuclear Hamiltonian in order to simplify the calculations and make the physical problems more tractable. This may have a considerable effect on the study of nuclear properties. For example, it was shown in Ref. [28] that the consequence of different Hamiltonians in PRM and cranking model on nuclear chaotic behavior might be of significance. The purpose of the present work is to show an alternative analysis on rotational damping by means of PRM, where angular momentum is strictly conserved and pairing correlation has been included explicitly. In what follows, individual nuclear levels and E2 transition properties from the region of discrete rotational bands into the regime of damped rotational motion are investigated in rare-earth nucleus  $^{168}\text{Yb}$  using particles-rotor model.

## II. FORMULATION

An even-even nucleus is visualized as an axially symmetric rotor with a few valence particles, which move more or less independently in the deformed potential of the core. The Hamiltonian of particles-rotor model is expressed as the sum of an intrinsic part and a collective part

$$H_{\text{PRM}} = H_{\text{intr}} + H_{\text{coll}}, \quad (1)$$

where  $H_{\text{intr}}$  describes microscopically the motion of valence particles near Fermi level and  $H_{\text{coll}}$  is the collective rotation of the core. The intrinsic Hamiltonian is taken as

$$H_{\text{intr}} = \sum_{j_1 m_1 j_2 m_2} \langle j_1 m_1 | -8\kappa\sqrt{\pi/5} Y_{20} | j_2 m_2 \rangle a_{j_1 m_1}^\dagger a_{j_2 m_2} - G \sum_{j' m' j m} a_{j' m'}^\dagger a_{j' \bar{m}'}^\dagger a_{j \bar{m}} a_{j m}, \quad (2)$$

where  $a_{j m}^\dagger$  and  $a_{j m}$  are the one-particle creation and annihilation operators. In order to describe the particle-hole excitations associated with rotational damping in realistic nuclei, the deformed mean-field of valence nucleons includes some different- $j$  shells. The single-

particle energy in the deformed mean-field is written as [28, 29, 30]

$$\sum_{j_1 m_1 j_2 m_2} \langle j_1 m_1 | -8\kappa \sqrt{\pi/5} Y_{20} | j_2 m_2 \rangle a_{j_1 m_1}^\dagger a_{j_2 m_2} = \sum_j \left\{ R_j + \sum_m \kappa \frac{3m^2 - j(j+1)}{j(j+1)} a_{jm}^\dagger a_{jm} \right\}, \quad (3)$$

where  $R_j$  is a parameter to indicate the relative energy between different- $j$  shells. The deformation parameter  $\kappa$  is related to the quadrupole deformation  $\beta$  through [27, 31]

$$\kappa \simeq 0.16 \hbar \omega_0 (N + 3/2) \beta, \quad (4)$$

where  $\hbar \omega_0$  is the harmonic oscillator frequency of the deformed potential and  $N$  the quantum number of the major shell. For example, in the case of  $i_{13/2}$  shell,  $k = 2.5$  approximately corresponds to  $\beta \sim 0.3$ , and  $h_{9/2}$  shell corresponds to  $k = 2.2$  MeV. The two-body correlation between valence nucleons is taken as pairing interaction with strength parameter  $G$ . Since we solve the two-body interaction exactly, it will contribute to both particle-particle channel and particle-hole channel.

The spin  $\vec{I}$  of nucleus is the sum of the angular momenta  $\vec{R}$  of core and  $\vec{J}$ , the sum of the angular momenta of valence nucleons. The collective Hamiltonian is expressed as

$$H_{\text{coll}} = \frac{R_1^2 + R_2^2}{2\mathcal{J}} = \frac{I^2 - I_3^2}{2\mathcal{J}} + \frac{J^2 - J_3^2}{2\mathcal{J}} - \frac{I_+ J_- + I_- J_+}{2\mathcal{J}}. \quad (5)$$

$H_{\text{rot}} = (I^2 - I_3^2)/2\mathcal{J}$  indicates the nuclear collective rotation. The recoil term  $H_{\text{rec}} = (J^2 - J_3^2)/2\mathcal{J}$  acts only on valence nucleons and contains one-body and two-body terms if there is more than one particle outside the core. Coriolis interaction  $H_{\text{cor}} = -(I_+ J_- + I_- J_+)/2\mathcal{J}$  is coupling the collective rotation and single particle motion of valence nucleons together.

The eigenfunctions of particles-rotor Hamiltonian can be expanded as

$$\Psi_{IM}^\alpha = \sum_K C_K^\alpha \varphi_{IMK}^\alpha \quad (6)$$

with the mixing coefficient  $C_K^\alpha$ , where the symmetric basis is given by

$$\varphi_{IMK}^\alpha = \sqrt{\frac{2I+1}{16\pi^2(1+\delta_{K0})}} \left\{ \mathcal{D}_{MK}^{I*}(\Omega) \phi_{K\alpha}^{(12\dots N)} + (-)^{I+K} \mathcal{D}_{M-K}^{I*}(\Omega) \phi_{K\alpha}^{(12\dots N)} \right\}. \quad (7)$$

$\mathcal{D}_{MK}^I(\Omega)$  is the usual rotation matrix and  $\phi_{K\alpha}^{(12\dots N)}$  the  $N$ -body anti-symmetrized wavefunction of valence nucleons.

The stretched E2 transition probability from an initial nuclear state  $\alpha$  at spin  $I+2$  to a final state  $\alpha'$  at  $I$  is calculated as

$$B(E2, \alpha I + 2 \rightarrow \alpha' I) = \frac{5}{16\pi} Q_0^2 M_{\alpha I+2, \alpha' I}^2, \quad (8)$$

with amplitude

$$M_{\alpha I+2, \alpha' I} = \sum_{KK'} C_K^\alpha (I+2) C_{K'}^{\alpha'} (I) \langle IK' 20 | I+2K \rangle \delta_{KK'}. \quad (9)$$

We neglect the minor contribution of non-collective  $E_2$  transition from valence nucleons since the intrinsic electric quadrupole moment  $Q_0$  is much larger than that from valence nucleons. The  $CG$  coefficient  $\langle IK' 20 | I+2K \rangle$  represents the coupling of the angular momenta in the intrinsic frame. The normalized  $E2$  transition probability  $S_{\alpha I+2, \alpha' I}$  is defined as

$$S_{\alpha I+2, \alpha' I} \equiv M_{\alpha I+2, \alpha' I}^2, \quad (10)$$

which satisfies  $\sum_{\alpha'} S_{\alpha I+2, \alpha' I} = 1$  from an initial state  $\alpha$  to many final states  $\alpha'$ .

### III. RESULTS AND DISCUSSIONS

The calculations presented below were carried out for rare-earth nucleus  $^{168}\text{Yb}$ , whose ground state has a stable elongated shape ( $\beta \sim 0.3$ ). For this nucleus there exists experimental data from the analysis of quasi-continuum gamma-spectra as well as data from discrete spectra identifying the rotational bands up to spin  $I \sim 40$  [32, 33]. In the framework of PRM, we consider nucleus  $^{168}\text{Yb}$  as a core  $^{160}\text{Yb}$  and eight valence neutrons moving in deformed mean-field. In order to provide a realistic description on many-particle many-hole excitations of the valence neutrons, according to the level scheme of Nilsson diagram [34], we include the subshells  $h_{9/2}$ ,  $i_{13/2}$ ,  $p_{3/2}$ ,  $f_{5/2}$  and  $p_{1/2}$  in the deformed mean-field. The relative energy  $R_j$  between different- $j$  shells is determined by Nilsson level diagram, e.g. it has been taken as about  $0.1\hbar\omega_0$  between shells  $h_{9/2}$  and  $i_{13/2}$ . The PRM calculations have been performed with the parameters: pairing strength  $G = 0.45$  MeV, the moment of inertia  $\mathcal{J} = 76.0 \hbar^2 \text{MeV}^{-1}$ ,  $\kappa = 2.5$  MeV for  $i_{13/2}$  intruder orbit and  $\kappa = 2.2$  MeV for other subshells included in the present calculation. These parameters have been used in earlier studies and are considered to be reasonable [19, 27, 28].

In our numerical calculation, the configuration space is spanned by various excitations of eight valence neutrons in the deformed mean-field. There exists off-diagonal Hamiltonian coming from pairing correlation, recoil term and coriolis interaction not only between the same- $j$  shell, but also from different- $j$  shells. These off-diagonal residual interactions cause the mixing of many-particle many-hole configurations. In carrying out the diagonalization

for each spin  $I = 0 - 60\hbar$ , the configuration truncation is done according to the excitation energy. The lowest 2000 basis states are included in the model diagonalization.

Fig. 1 displays the calculated energy levels with small horizontal bars for nucleus  $^{168}\text{Yb}$ . Strong E2 transitions satisfying condition  $S_{\alpha I+2, \alpha' I} > 1/\sqrt{2}=0.707$  are plotted with solid lines. Weaker transitions defined by condition  $0.5 < S_{\alpha I+2, \alpha' I} < 0.707$  are presented with dashed lines. One may observe that most of the strong E2 transitions lies in the region near yrast line, where the rotational band structures are identified. At higher excitation energy the transitions become much weaker and E2 transition from an initial state may spread out over many final states, implying the disappearance of rotational band structure.

In the experiments, strong E2 transitions are observed as discrete peaks in the gamma-ray spectra and the rest of transitions shows up as quasi-continuum spectra which contain transitions summed over many final states. For such a situation, it is useful to represent the E2 transition properties by means of strength distribution function. The strength function for a state  $\alpha$  at spin  $I + 2$  is given by [19]

$$S_{\alpha, I+2}(E_\gamma) = \sum_{\alpha'} S_{\alpha I+2, \alpha' I} \delta(E_\gamma - E_{\alpha I+2} + E_{\alpha' I}). \quad (11)$$

The fragmentation of E2 strength function is the rotational damping phenomenon. In order to quantify the onset of rotational damping, the branch number is defined as

$$n_{\text{branch}}(\alpha I + 2) \equiv \left( \sum_{\alpha'} S_{\alpha I+2, \alpha' I}^2 \right)^{-1}. \quad (12)$$

It counts effectively the branch number of E2 transitions from an initial level  $\alpha$  at  $I + 2$  to the final states  $\alpha'$ , which are allowed by the selection rules of the gamma-ray radiation. For a case where a given state decays to only one state at the lower spin,  $n_{\text{branch}}$  is equal to one. If there are two possible transitions with equal probability, the branch number is equal to two. In other words,  $n_{\text{branch}} < 2$  implies that the transition from a given state mainly decays to one final state, where the discrete rotational band structure is identified. In contrast,  $n_{\text{branch}} > 2$  states that the transitions spread over two or more final states, where the rotational damping takes place.

In order to indicate the E2 transition properties more precisely, the strength function  $S_{\alpha, I}(E_\gamma)$  is shown in Fig. 2 for the lowest 9 levels with  $I^\pi = 30^+$ . The branch number  $n_{\text{branch}}$  and excitation energy  $U$  are put for each level. The E2 transition associated with the first  $30^+$  state exhausts most of the total strength at gamma-ray energy 0.92 MeV. The

$30_2^+$ ,  $30_3^+$ ,  $30_4^+$  and  $30_5^+$  levels show essentially the same E2 distributions except for slight differences in the gamma-ray energy. The E2 decays from the  $30_6^+$ ,  $30_7^+$ ,  $30_8^+$  and  $30_9^+$  states display a different E2 strength distribution, being fragmented over several transitions, each of which carries a rather weak strength. Fig. 3 displays the quantity  $S_{\alpha,I}(E_\gamma)$  associated with the levels  $30_{35}^+$  and  $30_{36}^+$  lying at excitation energy  $U \sim 2.3$  MeV, and the levels  $30_{97}^+$  and  $30_{98}^+$  lying at  $U \sim 3.1$  MeV. The E2 strength distribution at  $U \sim 2.3$  MeV has about 16 branches, while the number of branches becomes around 42 at  $U \sim 3.1$  MeV. It indicates that the degree of the mixing between many-particle many-hole configurations becomes stronger as excitation energy increases, which is the basic mechanism to form the damping of collective rotational motion.

As the excitation energy increases, the rotational band structure gradually disappears and rotational damping takes place. Branching number is a key quantity to measure where rotational damping takes place and the degree of configuration mixing. The dependence of branching number on excitation energy is shown in Fig. 4 for spin (a)  $I^\pi = 20^+$ , (b)  $I^\pi = 30^+$  and (c)  $I^\pi = 40^+$ . The histogram gives the average branch number within the energy bins. One may observe that branching number increases with excitation energy. Using the criterion  $n_{\text{branch}} = 2$  for the onset of rotational damping, the onset energy is predicted to be around excitation energy  $U \sim 1.1$  MeV above yrast line. The onset energy in present calculation is similar with the theoretical prediction  $U \sim 0.8$  MeV in cranked Nilsson mean-field combined two-body residual interaction [19].

It should be noted, although the onset energy defined by condition  $n_{\text{branch}} = 2$  tells approximately where the rotational damping takes place, the transition from the region of rotational bands to rotational damping is not very sharply at the onset energy, but develops gradually as the excitation energy increases. As shown in Fig. 1, there exist some rotational bands in the region of rotational damping, where the excitation energy is higher than the onset energy. These band structures are surrounded by levels which do not have strong transitions. This indicates that the rotational band structure partly remains even in the region of rotational damping. Such feature of rotational bands is also displayed in Fig. 4. It is seen that there exist levels whose branching number is smaller than 2 at higher excitation energy.

Due to the onset of rotational damping, the number of rotational bands existing in a given nucleus is thus limited and gives a quantitative measure of rotational damping. Here,

the number of rotational bands corresponds to the experimental effective number of paths which can be obtained from  $E_\gamma \times E_\gamma$  spectrum by the fluctuation analysis method [8, 9]. Theoretically the number of rotational bands is defined by the number of levels with strong E2 transition, which satisfies conditions  $S_{\alpha I+2, \alpha' I} > 0.707$  or  $n_{\text{branch}} < 2$  with at least two consecutive steps  $I+2 \rightarrow I \rightarrow I-2$  of E2 decays [19]. Fig. 5 shows the calculated number of rotational bands as well as the experimental effective number of paths [9] for nucleus  $^{168}\text{Yb}$ . The solid line represents the results with the criterion  $S_{\alpha I+2, \alpha' I} > 0.707$  while the dashed line is calculated with condition  $n_{\text{branch}} < 2$ . The horizontal axis denotes the average gamma-ray energy  $E_\gamma = (E_{\gamma_1} + E_{\gamma_2})/2$ , where  $E_{\gamma_1}$  is the transition energy of  $I+2 \rightarrow I$  and  $E_{\gamma_2}$  for the transition  $I \rightarrow I-2$ . It is clear that the two conditions give essentially the same number of rotational bands around 30, and the theoretical calculations agree rather well with the experimental results in all the gamma-ray energy range.

In order to study the effect of pairing correlation between valence neutrons on rotational damping, Fig. 6 displays the calculated number of rotational bands with and without pairing correlation, together with experimental results. The solid line represents the results without pairing interaction between valence neutrons, while the dashed line is with the standard pairing  $G = 0.45$  MeV. The criterion  $S_{\alpha I+2, \alpha' I} > 0.707$  has been used to obtain the number of rotational bands. It is seen that the calculated number of bands becomes much larger when the pairing is turned off. In other words, the rotational band structure has strengthened and rotational damping has weakened when pairing  $G = 0.0$  MeV. This indicates that pairing correlation has a significant effect on the damping of rotational motion.

It should be mentioned that pairing correlation between valence neutrons has contributions to both diagonal and off-diagonal Hamiltonians. Diagonal Hamiltonian characterizing the property of mean-field favors the rotational band structure and retards the rotational damping, whereas the off-diagonal Hamiltonian characterizing the quantum fluctuations coming from residual interaction causes the mixing of many-particle many-hole configurations and prefers the rotational damping. Therefore, the delicate balance between the competition of diagonal and off-diagonal components of pairing correlation has determined the appearance of rotational damping. It is concluded that the off-diagonal components of pairing correlation (two-body residual interaction) play an important role in the appearance of rotational damping.

## IV. CONCLUSIONS

In order to provide a description of levels and E2 transitions in rapidly rotating nuclei with excitation energy up to a few MeV, we discussed the damping of collective rotational motion in rare-earth nucleus  $^{168}\text{Yb}$  by means of PRM with strict angular momentum conservation. It is found that rotational damping takes place at about 1.1 MeV above yrast line, and the number of levels which form rotational band structure is thus limited. The onset energy in the PRM calculation is similar with the theoretical prediction of the cranked Nilsson mean-field combined two-body residual interaction. The calculated number of rotational bands around 30 is in good agreement with experimental results in the gamma-ray energy range. The onset of rotational damping takes place quite gradually as a function of excitation energy. Even in the region of rotational damping, there still remains part of discrete rotational band structure. It is found that the calculated number of bands becomes much larger in the case of pairing strength  $G = 0.0$  MeV. The role of off-diagonal pairing correlation is emphasized. Hence, the pairing correlation between valence particles has significant effect on the appearance of rotational damping.

### Acknowledgments

This work was supported in part by the Japan Society for the Promotion of Science (JSPS) and the China National Natural Science Foundation (CNSF) as the bilateral program between Japan and China. E. G. Zhao acknowledges the support by Natural Science Foundation of China under Grant No. 10375001, the China Major Basic Research Development Program under Grant No. G2000-0774-07, the Knowledge Innovation Project of the Chinese Academy of Sciences under Grant No. KJCX2-SW-N02.

---

- [1] G. A. Leander, Phys. Rev. **C 25** (1982) 2780.
- [2] B. Lauritzen, T. Døssing and R. A. Broglia, Nucl. Phys. **A 457** (1986) 61.
- [3] J. C. Bacelar, G. B. Hagemann, B. Herskind, B. Lauritzen, A. Holm, J. C. Lisle and P. O. Tjøm, Phys. Rev. Lett. **55** (1985) 1858.

[4] J. E. Draper, E. L. Dines, M. A. Deleplanque, R. M. Diamond and F. S. Stephens, Phys. Rev. Lett. **56** (1986) 309.

[5] F. S. Stephens, J. E. Draper, J. L. Egido, J. C. Bacelar, E. M. Beck, M. A. Deleplanque and R. M. Diamond, Phys. Rev. Lett. **57** (1986) 2912.

[6] F. S. Stephens, J. E. Draper, J. C. Bacelar, E. M. Beck, M. A. Deleplanque and R. M. Diamond, Phys. Rev. Lett. **58** (1987) 2186.

[7] F. S. Stephens, J. E. Draper, M. A. Deleplanque, R. M. Diamond and A. O. Macchiavelli, Phys. Rev. Lett. **60** (1988) 2129.

[8] B. Herskind, A. Bracco, R. A. Broglia, T. Døssing, A. Ikeda, S. Leoni, J. Lisle, M. Matsuo and E. Vigezzi, Phys. Rev. Lett. **68** (1992) 3008.

[9] T. Døssing, B. Herskind, S. Leoni, M. Matsuo, A. Bracco, R. A. Broglia, and E. Vigezzi, Phys. Rep. **268** (1996) 1.

[10] B. Herskind, T. Døssing, S. Leoni, M. Matsuo and E. Vigezzi, Prog. Part. Nucl. Phys. **28** (Pergamon, 1992) p.235.

[11] B. Herskind, T. Døssing, D. Jerrestanm, K. Schiffer, S. Leoni, J. Lisle, R. Chapman, F. Khazaie and J. N. Mo, Phys. Lett. B **276** (1992) 4.

[12] B. Herskind, T. Døssing, S. Leoni, M. Matsuo N. Nica, D. C. Radford and P. Rasmussen, Nucl. Phys. **A 557** (1993) 191c.

[13] S. Leoni, B. Herskind, T. Døssing, P. Rasmussen, P. Bosetti, A. Bracco, R. Broglia, S. Frattini, M. Matsuo, N. Nica, E. Vigezzi, A. Atac, M. Bergström, A. Brockstedt, H. Carlsson, P. Ekström, F. Ingebretsen, H. J. Jensen, J. Jongman, G. B. Hagemann, R. M. Lieder, T. Lönnroth, A. Maj, B. Million, A. Nordlund, J. Nyberg, M. Piiparinen, H. Ryde, M. Sugawara, P. O. Tjøm and A. Virtanen, Nucl. Phys. **A 587** (1995) 513.

[14] S. Frattini, A. Bracco, S. Leoni, F. Camera, B. Million, N. Blasi, G. Lo Bianco, M. Pignanelli and E. Vigezzi et al., Phys. Rev. Lett. **83** (1999) 5234.

[15] F. S. Stephens, M. A. Delephanque, I. Y. Lee, D. Ward, P. Fallon, M. Cromaz, R. M. Clark, R. M. Diamond, A. O. Macchiavelli and K. Vetter, Phys. Rev. Lett. **88** (2002) 142501.

[16] T. Guhr and H. A. Weidenmüller, Ann. Phys. **A 193** (1989) 489.

[17] J. L. Egido and A. Faessler, Z. Phys. **A 339** (1991) 115.

[18] M. Matsuo, T. Døssing, E. Vigezzi, R. A. Broglia, Phys. Rev. Lett. **70** (1993) 2694.

[19] M. Matsuo, T. Døssing, E. Vigezzi, R. A. Broglia and K. Yoshida, Nucl. Phys. **A 617** (1997)

1.

- [20] M. Matsuo, T. Døssing, E. Vigezzi, S. Åberg Nucl. Phys. **A 620** (1997) 296.
- [21] K. Yoshida, M. Matsuo, Nucl. Phys. **A 612** (1997) 26.
- [22] K. Yoshida, M. Matsuo, Nucl. Phys. **A 636** (1998) 169.
- [23] M. Matsuo, K. Yoshida, T. Døssing, E. Vigezzi and R. A. Broglia, Nucl. Phys. **A 649** (1999) 379.
- [24] T. Døssing, B. Herskind, M. Matsuo, S. Leoni, A. Bracco, E. Vigezzi and R. A. Broglia, Nucl. Phys. **A 682** (2001) 439.
- [25] K. Yoshida, M. Matsuo, Y. R. Shimizu, Nucl. Phys. **A 696** (2001) 85.
- [26] S. Åberg, Phys. Rev. Lett. **64** (1990) 3119.
- [27] J. A. Sheikh and Y. Sun, Nucl. Phys. **A 733** (2004) 67.
- [28] A. T. Kruppa and K. F. Pái, Phys. Rev. **C52** (1995) 1818.
- [29] I. Hamamoto, Nucl. Phys. **A 271** (1976) 15.
- [30] R. Bengtsson and H. Hakansson, Nucl. Phys. **A 357** (1981) 61.
- [31] J. A. Sheikh, D. D. Warner, P. Van Isacker, Phys. Lett. **B 433** (1998) 16.
- [32] A. Fitzpatrick, S. A. Araddad, R. Chapman, J. Copnell, F. Lind'en, J. C. Lisle, A. G. Smith, J. P. Sweeney, D. M. Thompson, W. Urban, S. J. Warburton, J. Simpson, C. W. Beausang, J. F. Sharper-Shafer, S. J. Freeman, S. Leoni and J. Wrzesinski, Nucl. Phys. **A 585** (1995) 335.
- [33] J. R. B. Oliveira, S. Frauendorf, M. A. Deleplanque, R. M. Diamond, F. S. Stephens, C. W. Beausang, J. E. Draper, C. Duyar, E. Rubel, J. A. Becker, E. A. Henry and N. Roy, Phys. Rev. **C47** (1993) R926.
- [34] P. Ring, P. Schuck, The Nuclear Many-Body Problem (Springer-Verlag, 1980).

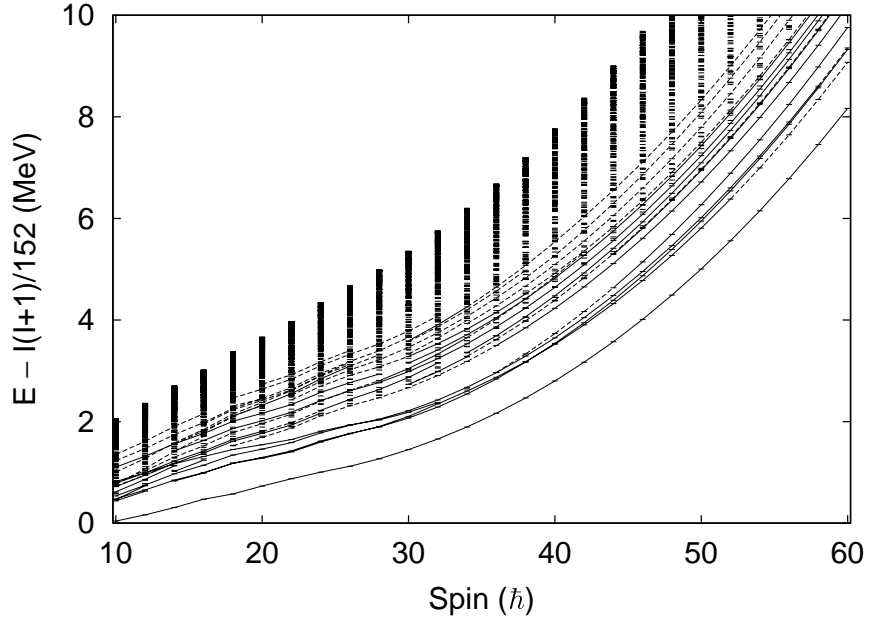


FIG. 1: The calculated energy levels are plotted with small horizontal bars for nucleus  $^{168}\text{Yb}$ . A reference energy  $I(I + 1)/2\mathcal{J}$  with  $\mathcal{J} = 76.0 \text{ } \hbar^2\text{MeV}^{-1}$  is subtracted. Solid lines connecting the energy levels represent the strong E2 transitions which have the normalized strength  $S_{\alpha I+2, \alpha' I}$  larger than 0.707. Dashed lines are the weaker E2 transitions with normalized strength between 0.5 and 0.707.

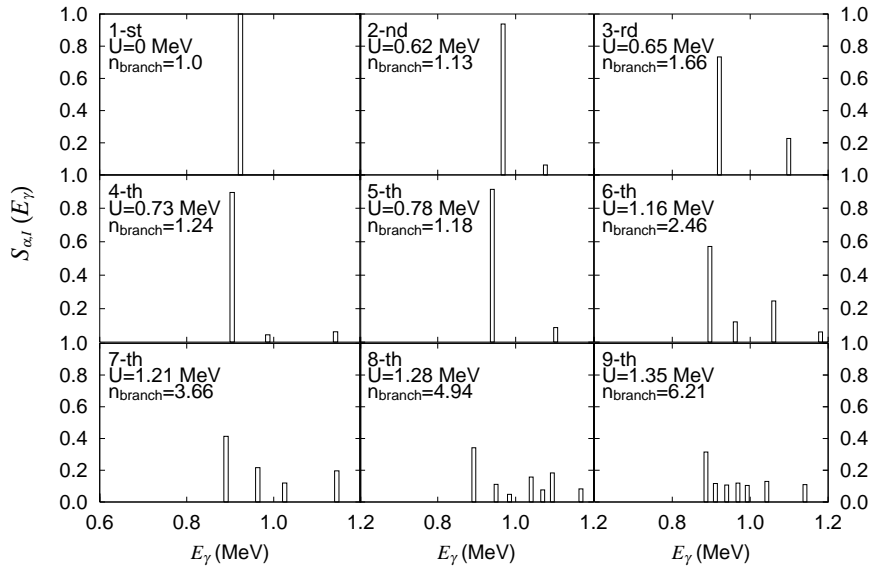


FIG. 2: The E2 strength distribution  $S_{\alpha,I}(E_{\gamma})$  from the lowest 9 levels with  $I^{\pi} = 30^{+}$ . The branch number  $n_{branch}$  and excitation energy  $U$  are put for each level.

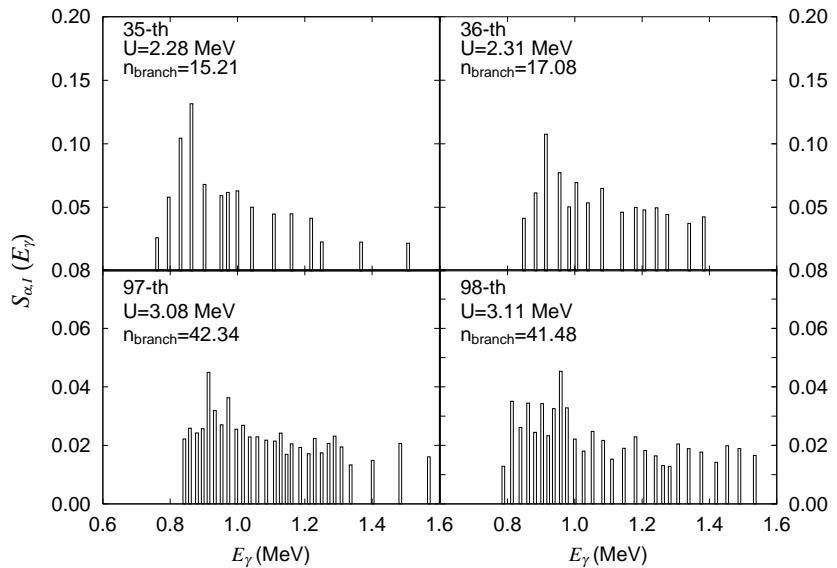


FIG. 3: The strength distribution  $S_{\alpha,I}(E_{\gamma})$  for the stretched E2 decays from the 35th and 36th, 97th and 98th excited levels with  $I^{\pi} = 30^{+}$ .

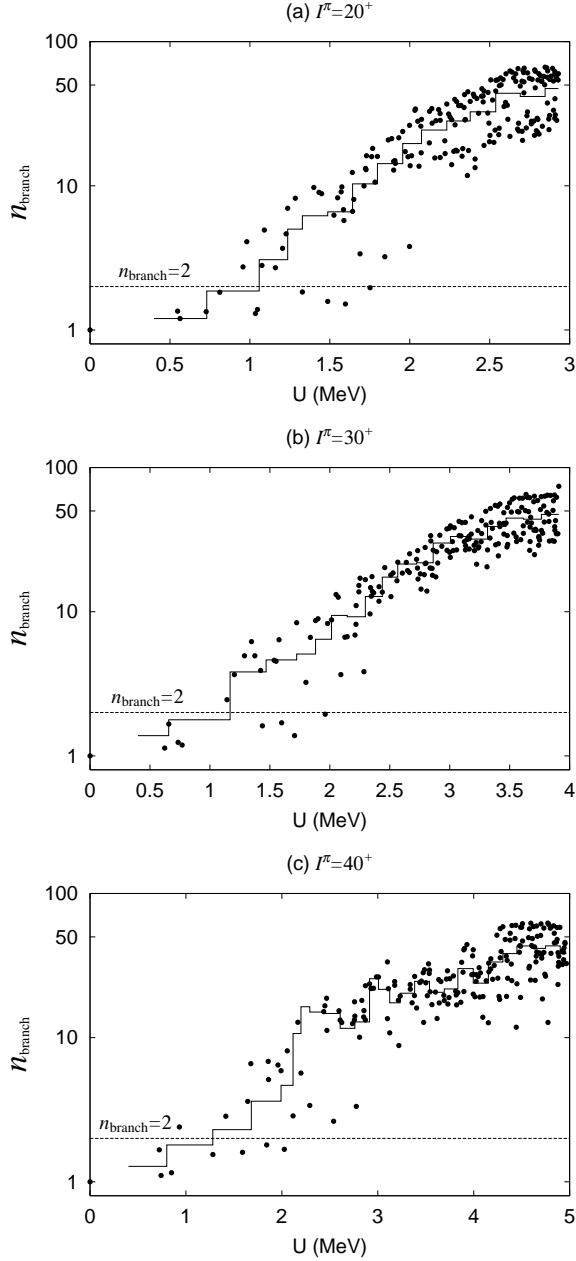


FIG. 4: The branching number  $n_{\text{branch}}$  for (a)  $I^\pi = 20^+$ , (b)  $I^\pi = 30^+$  and (c)  $I^\pi = 40^+$  as a function of excitation energy  $U$ . The histogram gives the average branch number within the energy bins. The horizontal line shows  $n_{\text{branch}}=2$  used to define the onset of rotational damping.

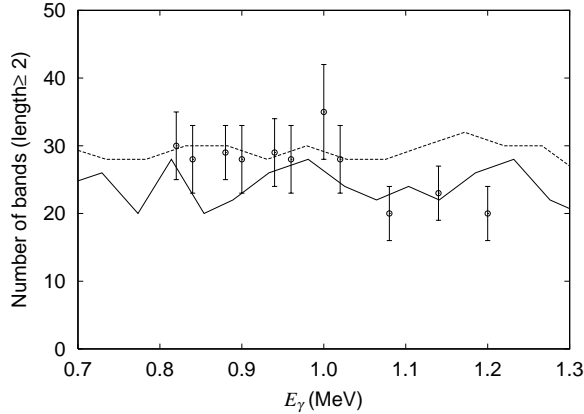


FIG. 5: The calculated number of bands is compared with the experimental effective number of paths [9] as a function of the average transition gamma-ray energy for nucleus  $^{168}\text{Yb}$ . The solid line is calculated with the criterion  $S_{\alpha I+2, \alpha' I} > 0.707$  while the dashed line represents the results with condition  $n_{\text{branch}} < 2$ .

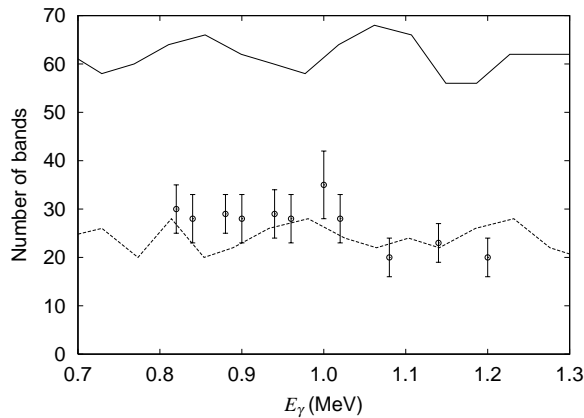


FIG. 6: The calculated number of bands with and without pairing interaction is compared with the experimental results as a function of the average gamma-ray energy. The solid line is the result with pairing strength  $G = 0.0$  MeV, while the dashed line is with the standard pairing  $G = 0.45$  MeV. The criterion  $S_{\alpha I+2, \alpha' I} > 0.707$  has been used to obtain the number of rotational bands.